

A REVIEW OF LUNAR AND PLANETARY MAGNETIC FIELD MEASUREMENTS
USING SPACE PROBES

by

Edward J. Smith

Jet Propulsion Laboratory

Pasadena, California

USA

GPO PRICE \$ _____

CFSTI PRICE(S) \$ _____

Hard copy (HC) 2.00

Microfiche (MF) 1.50

653 July 65

Introduction

In the six years from 1959 to 1965 the first phase in the magnetic exploration of the moon and the accessible planets, Venus and Mars, has been completed. It is no surprise to members of a conference such as this that magnetic field experiments were among the first scientific investigations of the moon and planets. The first space probe launched by the United States (Pioneer 1, October 1958) contained a magnetometer intended to investigate the lunar magnetic field. Unfortunately, Pioneer 1 only went about one-fifth of the distance to the moon before falling back to earth. However, in the intervening years, magnetic measurements have been successfully carried out near the moon, by Lunik 2 (September 1959), near Venus, by Mariner 2 (December, 1962), and near Mars, by Mariner 4 (July, 1965). What have we learned about the magnetic properties of the earth's nearest neighbors?

N66 29372
(ACCESSION NUMBER)
37
(PAGES)
OR-67604
(NASA CR OR TMX OR AD NUMBER)


FACILITY FORM 502

(THRU) _____
(CODE) _____
30
(CATEGORY)

Undoubtedly, most of you are aware that no fields were detected that could be attributed to either the moon or the two planets. The interpretation of the measurements could have been a relatively simple matter if a planetary magnetic field had been observed. The kind of information that we would all like might then have been available, such as the strength and orientation of the field, whether the source was predominantly a dipole or not and if it was, how it was directed with regard to the planetary rotation axis. However, a negative result means that the best we can do at present is to place an upper bound on the respective magnetic dipole moments. [The derivation of these bounds forms the basic content of this review.

In order to do a reasonably thorough job it will be necessary to consider not only the data obtained but also the spacecraft trajectory and even some of the instrument characteristics. [Moreover, planetary magnetic fields interact with the ionized interplanetary medium in a complicated manner, and in order to interpret the results it will be necessary to use the methods of plasma physics as well as the results of magnetic measurements made near the earth by space probes and satellites.]

For those who are in some field that is unrelated to plasma physics, I hasten to add that certain simplifications are possible. First, since neither Lunik nor the Mariners passed behind the moon or the planets, it will be unnecessary to discuss in much detail the planetary magnetic tail (see below). Second, the discussion will be based almost entirely on the empirical description of the solar wind-planetary field interaction



derived from near earth measurements with only passing reference to the basic theoretical concepts. Finally, our quite restricted objective will be to estimate the planetary dipole moment using our knowledge of how far certain features of the geomagnetic field stick out into interplanetary space.

Review of Near-Earth Measurements

The solar wind is the hot, outermost portion of the sun's corona which, instead of being in hydrostatic equilibrium with the gravitational field, is continuously expanding radially outward into interplanetary space. As it flows past a planet, the solar wind, acting as a fully ionized gas or plasma, tends to resist the penetration into it of the planetary magnetic field. The hydrodynamic wind pressure, which is equivalent to the momentum flux associated with its directed motion, compresses the planetary field into a tear drop-shaped cavity with a tail pointing away from the sun (figure 1). Inside the sunlit hemisphere of this cavity and throughout a nearly symmetric volume in the antisolar helisphere, the energy density of the compressed magnetic field exceeds the energy density of whatever particles are present inside the cavity such as the ionized outer atmosphere of the planet or trapped high energy radiation. This doughnut-shaped region is called the magnetosphere and its outermost sunlit boundary, on the opposite side of which is the solar wind, is called the magnetopause. At the subsolar point, the distance from the earth's center to the magnetopause is very near 10 earth radii (r_E) (Cahill and Amazeen, 1963). High latitude magnetic field lines on both the

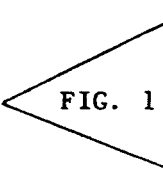


FIG. 1

sunlit and dark hemispheres of the earth are carried or dragged downstream by the wind to form an elongated magnetic tail (Smith, 1962; Cahill, 1964; Ness, 1965). The length of this tail is unknown at present. It trails downwind at least $30 r_E$ and may extend into interplanetary space hundreds or even thousands of earth radii.

Besides being fully ionized, the solar wind has two other characteristics that affect its interaction with the planets: 1) Because it carries along a weak ($\sim 5 \cdot 10^{-5}$ gauss = 5 γ) magnetic field (which started out at the sun as a coronal field), the solar wind behaves like a fluid. 2) The wind is hypersonic, i.e., the velocity of the plasma is much larger than the velocity with which waves can propagate through it. When the wind has to flow around an obstacle like the magnetosphere of a planet, these two characteristics cause a shock wave to occur upstream of the planet, somewhat like the bow wave that accompanies a boat (Axford, 1962; Kellogg, 1962; Spreiter and Jones, 1963). Figure 1 shows the hydromagnetic shock which is detached from the blunt magnetosphere. The shock front is stationary in the planetary frame of reference so that the situation is much like that encountered in aerodynamic wind tunnels or hydrodynamic channel flows where the medium moves rapidly past a model. Near the earth the shock front is located at a geocentric distance of $\sim 13 r_E$ on the sun line, and it flares out to $\sim 20 r_E$ along the dawn-sunset line (Ness, Searce, and Seek, 1964).

The shock front represents a second boundary with the interplanetary plasma and field on one side and a zone of irregular or turbulent

magnetic fields and plasma on the other. On approaching the earth, the position of the shock is detectable as an abrupt change from relatively quiet interplanetary conditions to a magnetically noisy condition which persists throughout the thick transition region or magnetosheath between the shock and the magnetopause. The shock front represents the outer boundary beyond which there is no observable effect due to a planetary field.

The characteristics of the fields in the magnetosphere and transition region are summarized in figure 2 which is an idealized plot of the field magnitude, $|B|$, as a function of geocentric distance in the direction toward the sun. The most important features are: 1) a region near the earth where the observed field in magnitude and direction is approximately the same as for the unperturbed geomagnetic field, 2) the magnetopause (at $10 r_E$), across which there is typically an abrupt change from a value about double the strength of the unperturbed field to the irregular transition region fields having average values of from 20 to 50 γ , and 3) the shock front at $13 r_E$ which may or may not exhibit an abrupt change from the average value of the interplanetary field ($\sim 5 \gamma$) to a larger average more typical of the transition region. These important features need to be kept in mind when we turn to a consideration of the space probe data.

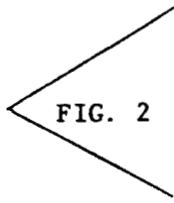


FIG. 2

Shape and Location of the Magnetopause and Shock Front for Other Planets

When no evidence of an intrinsic magnetic field is seen at

some position near the moon or a planet, the dipole moment may be estimated by considering how strong it could be without producing an observable perturbation of the solar wind. Of course, the orientation of the dipole moment is unknown and some direction for it must be assumed. In the following discussion we will assume that the dipole moment, \underline{M} , lies in the plane containing the solar wind velocity vector, \underline{V}_w , and the axis of rotation of the planet and that \underline{M} is also perpendicular to \underline{V}_w . The shape and location of the magnetopause and shock front under this condition have been investigated rather extensively by theorists since it approximates the situation near the earth. It is considered unlikely that a radically different orientation for \underline{M} , such as parallel to \underline{V}_w , would change things qualitatively; and it seems plausible that using the above assumptions the upper bound on $|\underline{M}|$ can be estimated to within at least a factor of 3.

An expression will now be derived for the distance from the magnetopause or the shock front to the center of a magnetized planet in terms of how far the corresponding feature is from the earth at a point of observation having the same sun-planet-spacecraft angle. As mentioned above, the effect that is detectable the furthest from the planet is the bow shock. Fortunately, the shape and location of both the earth's magnetopause and the bow shock surrounding the earth have been determined empirically by satellite and space probes. Their shape and location agree reasonably well with theoretical expectations.

The magnetopause and shock front are expected to be approximately surfaces of revolution having the direction from the sun to the planet

as axis (neglecting aberration due to orbital motion around the sun which rotates this axis $\sim 6^\circ$ for the earth and moon. According to various theoretical analyses (Midgley and Davis, 1963; Spreiter and Hyett, 1963; Mead and Beard, 1964; Slutz and Winkelman, 1964), the subsolar half of the magnetopause may be expressed as $R = r_o \cdot F(\psi)$, where the distance to the sub-solar point from the planet's center is $r_o = \left(\frac{KM^2}{P}\right)^{\frac{1}{6}}$ and ψ is the angle between the vector from the sun to the planet and the radius vector to the point of observation. In the above expression for r_o , M is the magnitude of the dipole moment while the solar wind momentum flux is $p = nmv_w^2$ with n the number density of protons having mass, m , and solar wind speed, v_w . Various constants have been absorbed in K which also incorporates a modest dependence on latitude that prevents the magnetopause from being strictly a surface of revolution. K will be assumed constant here since concern with latitude dependence is equivalent to questioning the orientation of \underline{M} . The shock front surface is determined by the size and shape of the magnetosphere and should exhibit essentially the same functional dependence. It follows from the above that at a given sun-planet-spacecraft angle the dipole moment of the planet (M) relative to the dipole moment of the earth (M_E) is related to the location of the magnetopause or shock front at the earth (R_E) and the planet (R) and to the solar wind pressures (P_E) and P):

$$\frac{M}{M_E} = \left(\frac{R}{R_E}\right)^3 \left(\frac{P}{P_E}\right)^{\frac{1}{2}} \quad (1)$$

The Lunar Magnetic Field

Lunik 2 impacted on the moon only one and one-half days after launch. The trajectory of Lunik 2 as it approached the moon at a fairly high latitude ($\sim 30^\circ$) is shown in figure 3 as a function of two parameters, the lunar radial distance and the sun-moon-spacecraft angle. The calculations on which the figure is based were carried out at the request of the author by Peter Feitis of the Jet Propulsion Laboratory using data presented in Sedov (1960). The spacecraft was not stabilized but tumbled through space (slowly rotating and precessing) so that the attitude was unknown after it left the dipole-like portion of the geomagnetic field. Triaxial magnetic field measurements were made by a fluxgate magnetometer inside the geomagnetic field, in cislunar space and just above the surface of the moon. The data obtained just before impact are shown in figure 4 along with the computed value of the total field (the root sum of the squares of the components) (Dolginov et al, 1960). The last datum was obtained at an altitude of 30 km.

The aspect of the data that most determines the upper bound on the lunar dipole moment is the sensitivity of the Lunik 2 magnetometer. In interpreting their data, the experimenters estimated that the instrument had a noise threshold of $\sim 100 \gamma$. This assessment is supported by the fact that no useful data were obtained near the earth beyond $\sim 7 r_E$ (the magnetopause and transition region were not detected) and apparent field changes as large as 100γ were observed in cislunar space in regions that should be like those where subsequent magnetometer measurements show relatively steady 5 to 10γ fields.

FIG. 3

FIG. 4

The upper fourth of figure 4 contains theoretical curves for three different values of the surface field assuming an inverse cube decrease with distance. The Lunik experimenters conclude that a surface field, B_s , as large as 100 γ could have escaped detection. This corresponds to an upper bound on M (equal to $B_s r_m^3$ with r_m the lunar radius) of $\sim 10^{-4} M_E$.

The above analysis weights the last few data points very heavily. It is interesting to consider where the magnetopause and shock front might have occurred since, as we have seen, a 100 γ field at the earth's magnetopause is adequate to balance the typical solar wind pressure. Using the equation (1) above and assuming $p = p_E$, for $M = 10^{-4} M_E$, $r_{om} = 10^{-\frac{4}{3}} \cdot 10 r_E = 1.7 r_m$. Since the location of the shock front is an additional 30% or so beyond the magnetopause, the shock front might occur at $2.2 r_m$ at the subsolar point. If the same equation is applied to the Lunik 2 trajectory and allowance is made for a sun-moon-spacecraft angle of $\sim 60^\circ$ during the approach, the magnetopause and shock front would have occurred at the position of the two arrows in figure 4. It is not surprising that no additional information about the dipole moment can be obtained since the field inside the magnetopause was assumed to be $\sim 100 \gamma$ and the transition region fields, if they are like the earth's, are even smaller and would be lost in the instrument noise.

The upper bound established by Lunik 2 still does not settle some interesting scientific questions, such as whether the moon could

accumulate a weak atmosphere from the solar wind (Nakoda and Mihalov, 1963). If the surface field is 100 γ then we would not expect a weak solar wind (at least a wind having the pressure measured by spacecraft during the minimum solar activity of the last few years) to reach the surface. However, if the surface field is only 10 γ then the solar plasma can readily penetrate to the surface. This would modify the nature of the interaction between the solar wind and the moon although a shock front and transition region are still expected (Gold, 1965). (However, simple extrapolation of the shape and location of the earth's shock front to the vicinity of the moon would then be a questionable procedure.) In this case a weak lunar field may exist that is not intrinsic to the moon, originating perhaps inside a molten core, but has been caused by diffusion of the interplanetary field into the solid conducting body of the moon (Gold, 1965). For values of the surface field between 10 and 100 γ conditions at the surface can be expected to be very changeable since the solar wind can show strong daily variations.

Magnetic Field of Venus

Mariner 2 passed within 41,000 km of the center of Venus on 14 December 1962. The encounter trajectory is shown in figure 5 in a Venus-centered coordinate system appropriate to the investigation of a possible magnetic cavity enclosing the planet (Smith, Davis, Coleman, and Sonett, 1965). The R axis points away from the sun (in the direction

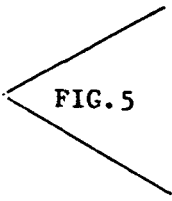


FIG. 5

of the solar wind), the T axis is parallel to the ecliptic plane and positive in the direction in which the planets move, and N, which is orthogonal to T and R, makes an angle of only $\sim 1.5^\circ$ with the north polar axis of the ecliptic. If Mariner 2 had encountered the earth, instead of Venus, on such a trajectory, it would have entered the transition region behind the earth at a geocentric distance of 150,000 to 200,000 km, the magnetosphere at 100,000 to 125,000 km, and would have passed outward through the magnetopause and shock front near the noon meridian. At closest approach (41,000 km), the earth's field has a magnitude of $\sim 125 \gamma$ and is relatively free of distortion by the compression of the field further out so that it would have been possible to estimate the three components of the dipole moment to within $\sim 10\%$.

Magnetic fields in the vicinity of Venus were measured continuously along the trajectory by a triaxial flux gate magnetometer. The sensing element of such a magnetometer is a cylinder of high permeability magnetic material that is driven into saturation by passing an audio frequency current through a set of primary windings. In the presence of a steady ambient magnetic field having a component parallel to the cylinder axis, the voltage induced in a set of secondary windings includes a second harmonic of the primary drive frequency. The amplitude of this second harmonic component is proportional to the magnitude of the steady field component, and its

phase relative to the drive signal is determined by whichever of the two possible directions the field component is pointing in. The three mutually orthogonal sensors were located on the Mariner super-structure (see fig. 6) as far as possible from the main body of the spacecraft (which contained the magnetometer electronics and the other experiments) in order to reduce the contribution of their magnetic fields to the measurements. Nevertheless, the spacecraft contributed a field at the sensor slightly in excess of 100 γ . Fortunately, there were no significant magnetic field changes associated with the spacecraft mode of operation near the planet.

FIG. 6

The Mariner 2 data system sampled the three magnetometer output voltages every 20 seconds for approximately 7 hours during encounter. The voltages were converted to digital data, 8-bit binary numbers lying between 0 and 255. The uncertainty introduced by the conversion, $\sim 2\frac{1}{2}$ γ per axis, was substantially larger than the $\frac{1}{2}$ to $\frac{1}{2}$ γ noise threshold of the magnetometer. The encounter data are shown in figure 7 as a succession of vertical lines whose length corresponds to the digitization uncertainty. The three field components, B_N , B_T , and B_R , correspond to the coordinate directions described above.

FIG. 7

A cursory inspection of the data shows no field changes that could be definitely attributed to Venus. If smooth, long period field changes that might be characteristic of a planetary field are investigated,

the largest such change that could be buried in the observations would have had a resultant magnitude of only 10 γ . However, if Mariner 2 had penetrated into the magnetosphere, a field of at least 100 γ should have been observed. We can safely conclude, therefore, that the spacecraft trajectory did not penetrate close enough to Venus to reach the magnetopause. Similarly, the shock front, the magnetic effect that could have been seen at the greatest distance from the planet, should appear in the data as an onset of enhanced field fluctuations with amplitudes of several gamma and periods ranging from a few seconds to several minutes or more. However, such fluctuations are clearly less than 3 to 5 γ on any axis and the amplitudes could be considerably less on at least two axes and be consistent with the analog-to-digital conversion uncertainty. Furthermore, one of the two quietest intervals occurred as Mariner traveled from 70,000 to 41,000 km (closest approach). When compared with interplanetary measurements made both before and after encounter, there is no difficulty in accepting the encounter measurements as typical interplanetary field data and concluding that they show no trace of the presence of Venus. This result is consistent with the Mariner 2 particle experiments which indicated that there was no perturbation of the solar wind associated with passage past Venus, (Neugebauer and Snyder, 1965), and no high energy radiation belts were detected (Frank, Van Allen, and Hills, 1963; Anderson 1963).

An upper bound on the magnetic dipole moment of Venus can be estimated using the relation derived above. This equation can be used to scale down the earth's shock front contour for various possible values of the dipole moment. For the limiting dipole moment the trajectory would have intersected the shock somewhat downstream of the position of closest approach in a direction approximately 105° from the sun-Venus line and at a distance $\sim 52,000$ km from Venus. Near earth the corresponding distance to the shock front at a sun-earth-spacecraft angle of 105° is $\sim 27.5 R_e$ or 175,000 km. This implies $\left(\frac{R}{R_E}\right)^3 = .026$. On the average, the solar wind pressure or momentum flux near Venus will be approximately one-half of its value at the earth's orbit since the proton number density, N , is inversely proportional to the square of the distance from the sun and the wind speed is nearly independent of distance. The Mariner 2 plasma experiment showed that the actual solar wind pressure was indeed approximately 2 times the typical solar wind pressure near the earth (Neugebauer and Snyder, 1965). This dependence on $\left(\frac{P}{P_E}\right)^{\frac{1}{2}}$ effectively increases the limiting dipole moment by a factor of ~ 1.4 so that $M \leq .036 M_E$.

The conclusion that Venus' dipole moment is only one-tenth to one-thirtieth of the earth's dipole moment is qualitatively consistent with the expectation, based on the dynamo theory of planetary magnetic fields, that Venus is rotating too slowly to generate a magnetic dipole field as large as the earth's. If M_V had been found to be approximately

equal to M_E , it could have implied that the core of Venus was somehow very different from the core of the earth or that the dynamo mechanism was less well understood than we suppose. Theorists have been spared such agony. The Mariner observations definitely rule out the suggestion that the magnetic field of Venus is large enough to affect the solar wind flow at a distance of 450 Venus radii (Houtgast and vanSluiter, 1962)

Since M_V is less than $0.1 M_E$, the cosmic ray flux above the atmosphere of Venus will be everywhere comparable to what is observed only above the earth's polar regions. A zone of trapped, high energy particles similar to the earth's is not excluded, but it will have to be confined within a magnetosphere having a radial extent of only 5 Venus radii or less.

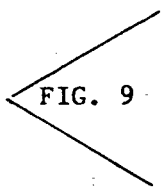
Magnetic Field of Mars

On July 14-15, 1965 Mariner 4 passed near Mars, being only 13,200 km ($3.9 r_M$) from the planet's center at closest approach. The flight path appears in Figure 8, again in a planet-centered, sun-oriented coordinate system. The R axis is radially outward from the sun, the T axis is parallel to Mars equatorial plane and positive in the direction of planetary motion, and the third orthogonal component, N, lies in the plane containing the sun vector (R) and Mars rotation axis with which it makes an angle of $\sim 25^\circ$. Mariner 4 did not pass into the planet's shadow but moved away in the direction of an asymptote corresponding to a local time of ~ 2200 hours. This feature has the



FIG. 8

important consequence that a planetary moment large enough to cause a magnetic tail reaching the Mariner trajectory after closest approach would have caused the magnetopause or shock front to intersect the trajectory before closest approach. Thus, the limit on the Martian dipole moment was set by the capability of the magnetometer to detect the shock front. Near earth, just after launch, the Mariner magnetometer data showed clear evidence of passage through the geomagnetic bow shock (Coleman, Smith, Davis, and Jones, 1965).

Mariner 4 (figure 9) carried a new type of vector magnetometer, the  FIG. 9 low field helium magnetometer. In this instrument circularly polarized infrared radiation from a helium lamp is focused on a cell containing metastable helium, and the resulting Zeeman absorption is monitored by an IR detector. By a process called optical pumping, absorption and reradiation quickly leads to a highly unequal population of helium atoms being in one of the Zeeman levels, one which cannot absorb the incident radiation so that absorption is inhibited and the gas becomes transparent. The pumping efficiency depends on the cosine squared of the instantaneous angle between the direction of the magnetic field and the optic axis consisting of the lamp, circular polarizer, cell and detector. A magnetic field rotating at 50 cps, generated at the cell by passing two sinusoidal currents 90° out of phase through a set of helmholz coils, produces a doubly periodic (100 cps) variation in the transparency. The presence of an ambient magnetic field causes a

50 cps component to appear in the detector output which is then demodulated and used to generate a steady current in the field coils to force the resultant steady field to zero. The use of feedback greatly improves the linearity and stability of the magnetometer output which consists of three steady analog voltages proportional to the three components of the ambient field. The noise threshold of the instrument is equivalent to only 0.1Γ rms, significantly less than the uncertainty of $\frac{1}{3} \Gamma$ introduced by in-flight analog to digital conversion. During encounter, four triaxial data samples were obtained every 50.4 seconds at intervals of 6.0, 3.6, 9.6, and 31.2 seconds.

None of the magnetometer data obtained near Mars were presented in the preliminary report on which this discussion is based, so none can be shown here (Smith, Davis, Coleman, and Jones, 1965). No definite magnetic effect associated with the planet was evident in the measurements. Fortunately the interval before, and during, encounter was one of relative magnetic calm. The seven months of interplanetary measurements showed a pattern of alternating disturbed and quiet intervals related to daily changes in solar activity. The search for irregular fields associated with the bow shock would have been more difficult if the interplanetary field had been disturbed rather than quiet. Irregular variations sometimes occur in interplanetary space that have the appearance of a hydromagnetic shock but that are undoubtedly caused by impulsive solar wind variations. However, for approximately seven hours preceding closest approach no changes in any

of the measured field components were observed that could not be readily identified as fluctuations of the interplanetary magnetic field. Approximately 20 minutes after closest approach a disturbance began with an abrupt jump of 5 γ that continued for almost 3 hours, after which the components returned to their previous values. This disturbance could have been one of many similar interplanetary disturbances, or it could have been a bow shock associated with a weak Martian magnetic dipole moment. In lieu of any evidence in the preliminary analysis to distinguish between these two possibilities, it will be assumed that the disturbance was actually a bow shock, and a conservative estimate of the upper bound on the Martian dipole moment will be derived.

The disturbance was seen at an areocentric distance of 14,700 km at a Sun-Mars-spacecraft angle of 110° . Near earth at the same angle, the IMP-1 and Mariner 4 data are consistent with the bow shock being located beyond $37.5 r_E$ or at 240,000 km. The plasma experiment indicates that the solar wind pressure was less than $\frac{1}{2} \cdot 10^{-8}$ dynes \cdot cm $^{-2}$ during the encounter with Mars (H. S. Bridge, A. Lazarus, and C. W. Snyder, private communication). Furthermore, a similar instrument on the earth satellite IMP-1 yielded a representative value of P_E equal to $2 \cdot 10^{-8}$ dynes cm $^{-2}$. When the foregoing information is substituted into the equation for M/M_E , the computed bound on M_M turns out to be $\sim 10^{-4} M_E$. This estimate is unlikely to be too low by as much as a factor of 3. On the other hand, if the disturbance seen just after closest approach was not associated with Mars the upper

bound on M_M will be even smaller. Therefore, it is safe to conclude that the Martian dipole moment is no larger than 1/3000 of the dipole moment of the earth. Of course, it could be essentially zero. Figure 10 shows the shock front near Mars (computed with M_M equal to 10^{-3} and $10^{-4} M_E$) and the Mariner trajectory which is plotted as a function of areocentric distance and the instantaneous Sun-Mars-spacecraft angle.

FIG. 10

The upper bound on the Martian dipole moment is dramatically smaller than the corresponding number derived for Venus using the Mariner 2 data. This improved sensitivity is the consequence of the closer approach of Mariner 4 to the planet and the greater sensitivity of the Mariner 4 magnetometer data.

The smallness of the Martian dipole moment is again consistent with the qualitative predictions of the dynamo theory. Since the rotation rates of Mars and the earth are nearly equal, a very small fluid core is indicated for Mars in agreement with earlier proposals (Urey, 1957; MacDonald, 1962; Lyttleton, 1965). The Martian interior appears to be more like the interior of the moon than the interior of the earth. A moment of $3 \cdot 10^{-4} M_E$ implies the magnetic field at the surface due to the dipole is no larger than $\sim 100 \gamma$. It also means that the flux of cosmic rays at the top of Mars atmosphere should everywhere be comparable to what is observed at the earth only above the polar regions. The magnetic energy density associated with a moment this small drastically limits the maximum energy density of

trapped particles so that only a very weak radiation belt will be possible. Since the magnetopause must lie inside an areocentric radius of $\sim 2.5 r_M$ at the subsolar point, the volume occupied by any radiation belt that may exist must also be small. This implication is consistent with the results of the Mariner 4 high energy particle experiments which did not detect any radiation near Mars (Simpson and O'Gallagher, 1965; Van Allen, et al, 1965).

ACKNOWLEDGMENTS

The Lunik 2 trajectory in the vicinity of the moon was computed by Peter Feitis (Jet Propulsion Laboratory).

~~THE NATIONAL AERONAUTICS AND SPACE ADMINISTRATION~~

~~SUPPORTED THIS RESEARCH UNDER CONTRACT NAS 44-71~~

This paper presents the results of one phase of research carried out at the Jet Propulsion Laboratory, California Institute of Technology, under Contract No. NAS7-100, sponsored by the National Aeronautics and Space Administration.

REFERENCES

- Anderson, H. R., J. Geophys. Res. 69, 2651 (1964).
- Axford, W. I., J. Geophys. Res. 67, 3791 (1962).
- Cahill, L. J. and P. G. Amazeen, J. Geophys. Res. 68, 1835 (1963).
- Cahill, L. J., I. G. Bull. 79, Trans. Am. Geophys. Union 45, 231 (1964).
- Coleman, P. J., Jr., E. J. Smith, L. Davis, Jr., and D. E. Jones, to appear in Space Research VI, proc. of 6th COSPAR Symposium (1965).
- Dolginov, S. S., E. G. Eroshenko, L. I. Zhuzgov, and N. V. Pushkov, A Study of the Magnetic Field of the Moon (Ed. Z. Kopal and Z. Mikhailov), Academic Press, New York (1960).
- Frank, L. A., J. A. Van Allen, and H. K. Hills, Science 139, 905 (1963).
- Gold, T., The Magnetosphere of the Moon, in The Solar Wind (Ed. R. J. Mackin, Jr. and M. Neugebauer) Pergamon (1965).
- Houtgast, J. and A. van Sluiter, Nature 196, 464 (1962).
- Kellogg, P. J., J. Geophys. Res. 67, 3805 (1962).
- Lyttleton, R. A., Mon. Not. Roy. Astron. Soc. 129, 21 (1965).
- MacDonald, G. J. F., J. Geophys. Res. 67, 2945 (1962).
- Mead, G. D., and D. B. Beard, J. Geophys. Res. 69, 1169 (1964).
- Midgley, J. E., and L. Davis, Jr., J. Geophys. Res. 68, 5111 (1963).
- Nakada, M. P., and J. D. Mihalov, J. Geophys. Res. 67, 1670 (1963).
- Neugebauer, M. and C. W. Snyder, J. Geophys. Res. 70, 1587 (1965).
- Ness, N. F., J. Geophys. Res. 70 2989 (1965).

- Ness, N. F., C. S. Searce, and J. B. See, J. Geophys. Res. 69, 3531 (1964).
- Sedov, L. I., The Orbits of Cosmic Rockets in the Direction of the Moon, Artificial Earth Satellites 5, (Ed. L. V. Kurnasova), Plenum Press, New York (1961).
- Simpson, J. A. and J. J. O'Gallagher, Science 149, 1233 (1965).
- Slutz, R. J. and J. R. Winkelman, J. Geophys. Res. 69, 4933 (1964).
- Smith, E. J., J. Geophysical Research 67, 2045 (1962).
- Smith, E. J., L. Davis, Jr., P. J. Coleman, Jr., and D. E. Jones, Science 149, 1241 (1965).
- Smith, E. J., L. Davis, Jr., P. J. Coleman, Jr., and C. P. Sonett, J. Geophys. Res. 70, 1571 (1965).
- Spreiter, J. R., and B. J. Hyett, J. Geophys. Res. 68, 1631 (1963).
- Spreiter, J. R. and W. P. Jones, J. Geophys. Res. 68, 3555 (1963).
- Urey, H. C., Phys. and Chem. Earth 2, 46 (1957).
- Van Allen, J. A., L. A. Frank, S. M. Krimigis, and H. K. Hills, Science 149, 1228 (1965).

FIGURE CAPTIONS

Figure 1

The division of space surrounding the earth into different magnetic regions. As indicated, the view is from above the earth's pole. The hypersonic streaming of the solar wind past the asymmetric magnetosphere sets up a bow shock wave. The figure is not drawn to scale and only simple, smooth surfaces have been employed.

Figure 2

Characteristic Magnetic Fields Near Earth. This is a composite of the typical field characteristics in the various magnetic regions viewed as a function of geocentric distance only.

Figure 3

Lunik 2 trajectory near the Moon. The selenocentric distance of Lunik 2 is plotted against the associated sun-moon-spacecraft angle. The two smooth contours showing the nominal locations of the shock front and magnetopause were scaled down from the corresponding contours for the earth.

Figure 4

Lunik 2 magnetometer data. The three components of the apparent field (mostly or entirely magnetometer noise) are shown along with T , the square root of the sum of the squares, for the last 4000 km of the flight. The dashed curves at the top represent magnetic

fields having different values at the surface and all falling off as the inverse cube of the selenocentric distance (Taken from Dolginov et al, 1960). Arrows at the top marked SF and MP mark the nominal location of shock front and magnetopause, respectively, assuming a lunar magnetic dipole moment of $10^{-4} M_E$.

Figure 5

Mariner 2 trajectory near Venus. The trajectory is shown in so-called cavity coordinates defined in the text. The aphrodiocentric distance at a specific GMT is indicated by the filled dots. (From Smith et al, 1965).

Figure 6

The Mariner 2 Spacecraft. The basic structure consists of a hexagonal body containing the engineering subsystems and experiment electronics to which were appended two solar panels, a directional antenna (the mesh paraboloid at the bottom), and a superstructure to support the omnidirectional antenna (inside the cylindrical insulator at the top) and science sensors, including the magnetometer. Mariner 2 was inertially stabilized (non-spinning) using the sun and earth as references.

Figure 7

Mariner 2 magnetometer data. The magnetic field measurements from 13 hours before, to 10 hours after, closest approach are shown. The data appear as a series of vertical lines representing the uncertainty

introduced by digitizing the data prior to their being telemetered. Vertical lines equivalent to field changes of 10γ are shown. The instantaneous distance to Venus appears at the bottom of two of the panels. (Smith et al, 1965).

Figure 8

Mariner 4 Trajectory Near Mars. This figure is comparable to figure 5; however, the R, T, N axes are defined slightly differently (see the text).

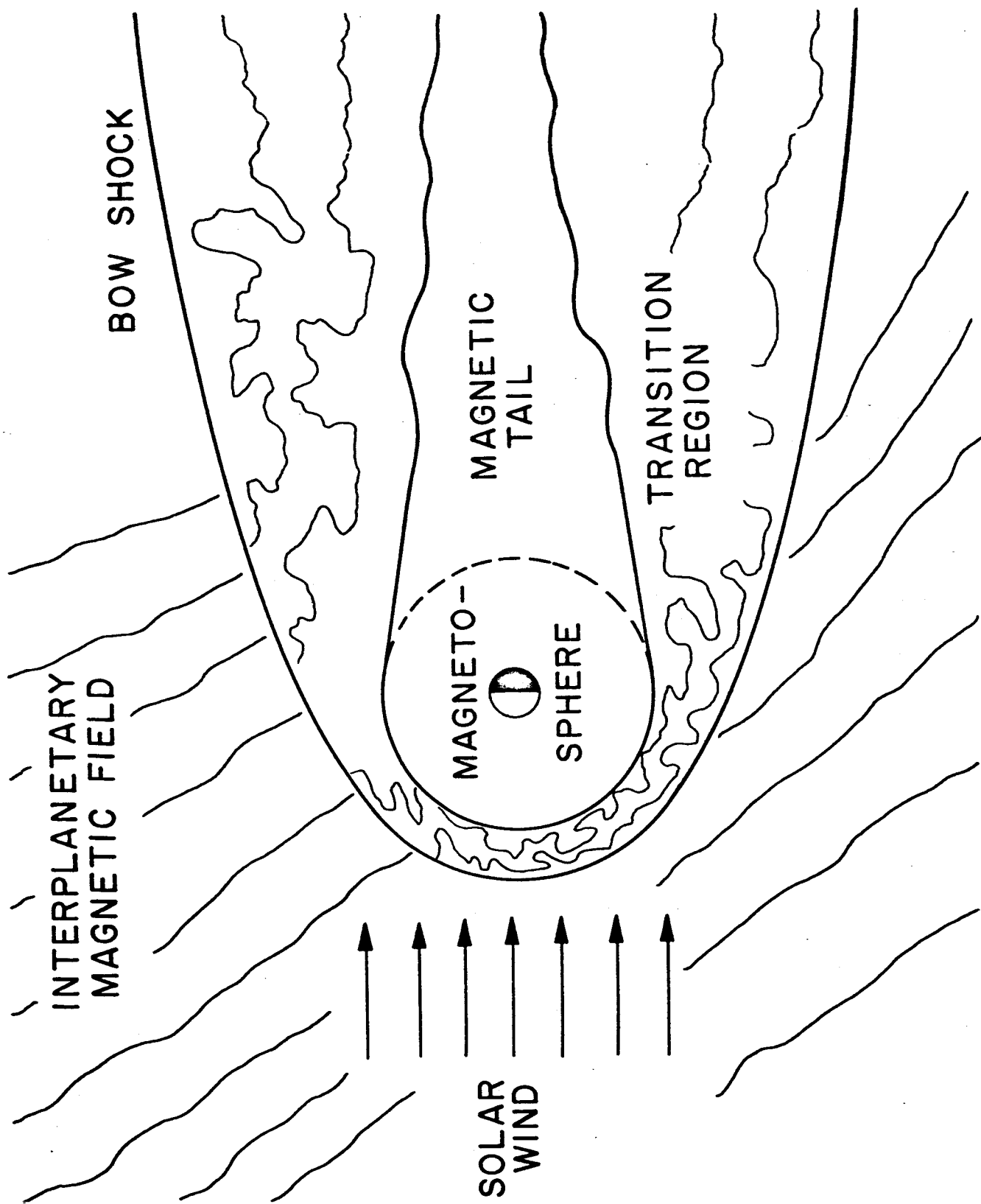
Figure 9

Mariner 4 Spacecraft. The octagonal body containing the engineering and scientific subsystems also supports the four solar panels (at the ends of which are attitude control vanes), a central directional antenna and a long wave guide ending in an omnidirectional antenna. The vector helium magnetometer sensor is the bright sphere closest to the upper end of the waveguide. The spacecraft was stabilized (non-spinning) using the sun and the star, Canopus, as references.

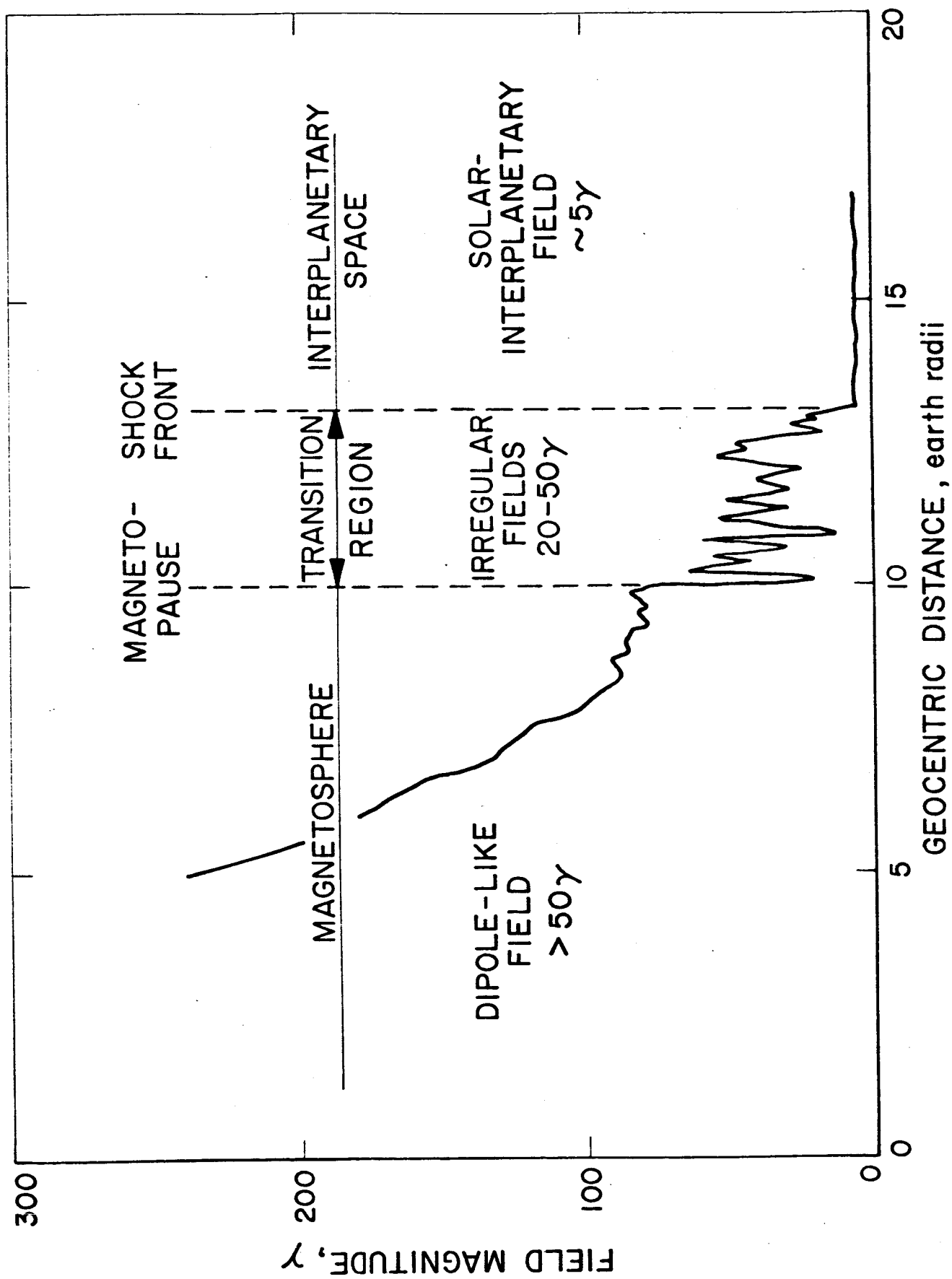
Figure 10

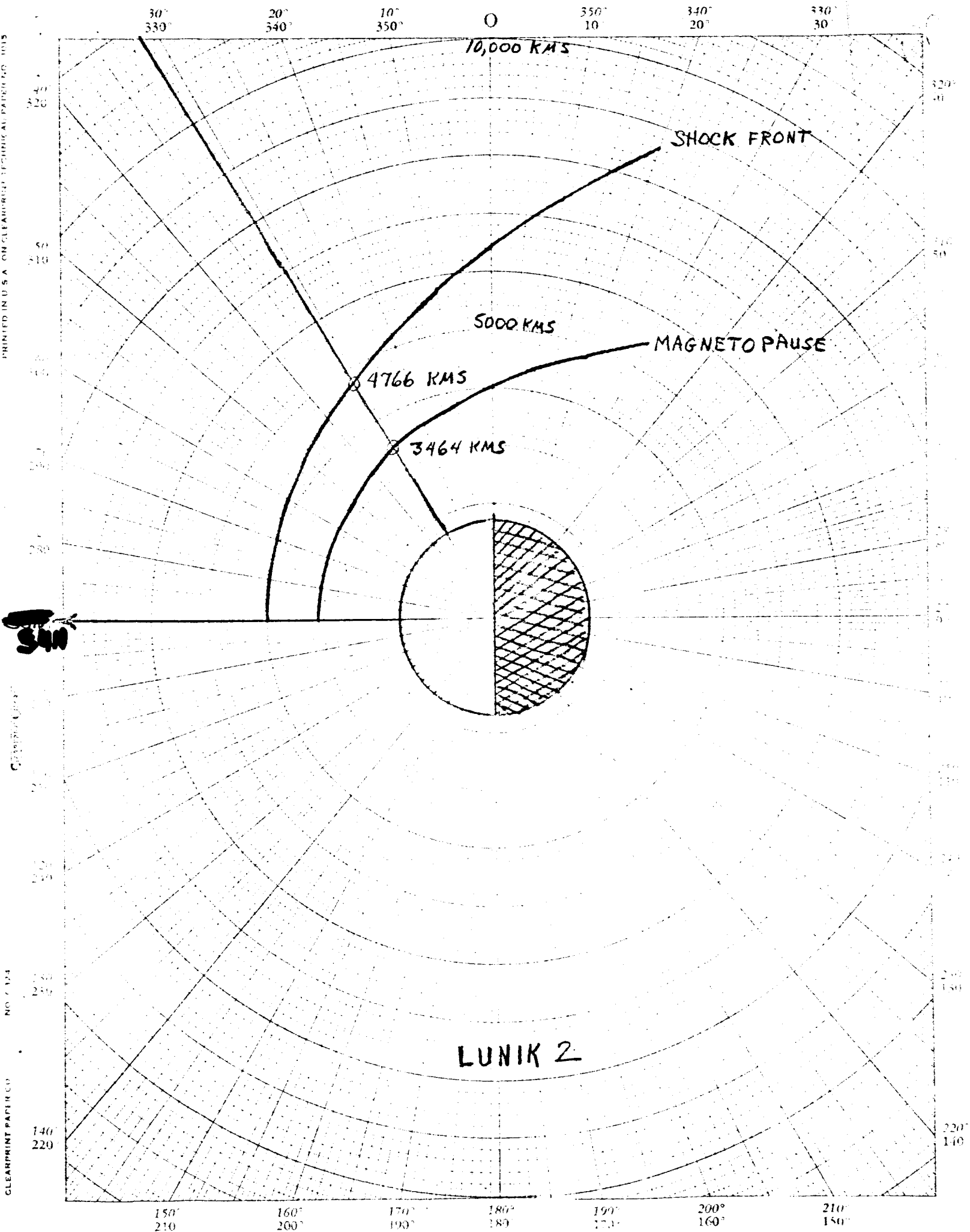
Mariner 4 Encounter Showing Possible Shock Fronts. The spacecraft trajectory is shown as a polar plot of areocentric distance versus the corresponding sun-Mars-spacecraft angle. Contours have been drawn for magnetic dipole moments of 10^{-3} and 10^{-4} times that of the earth using the scaling relation discussed in the text. Their irregularity is

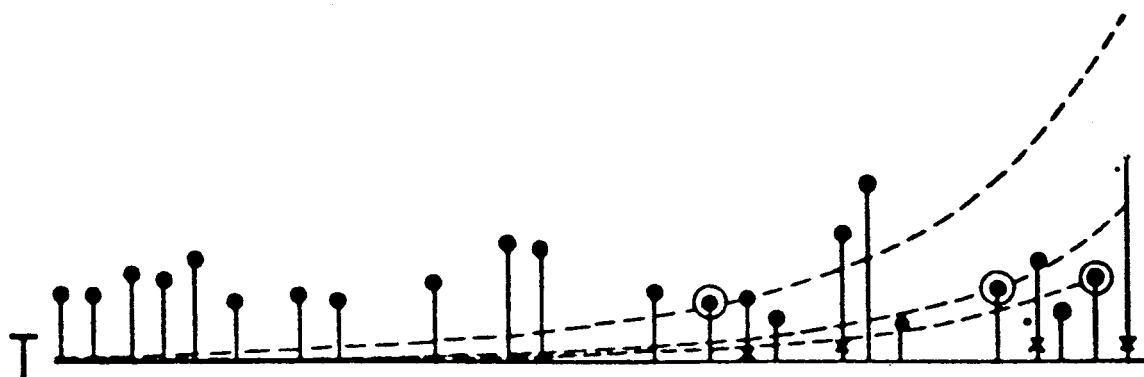
a reminder that the actual shock front location near earth fluctuates with irregularities in the solar wind. The intersection of the innermost contour with the trajectory corresponds to the onset of a magnetic disturbance.



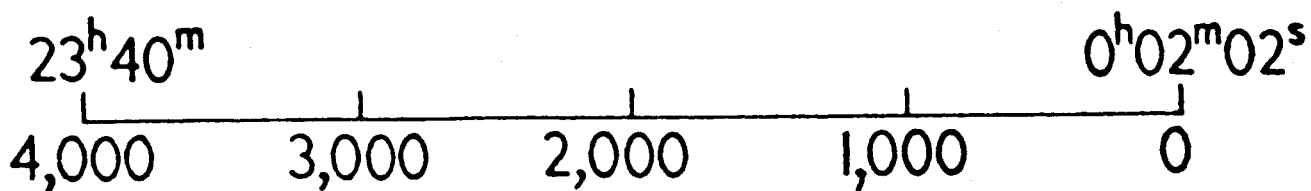
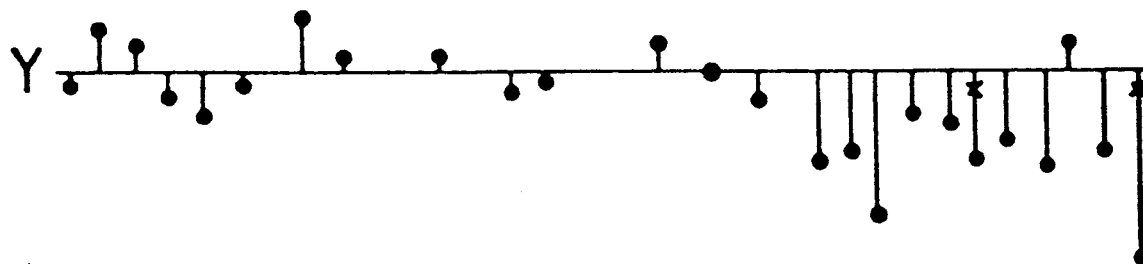
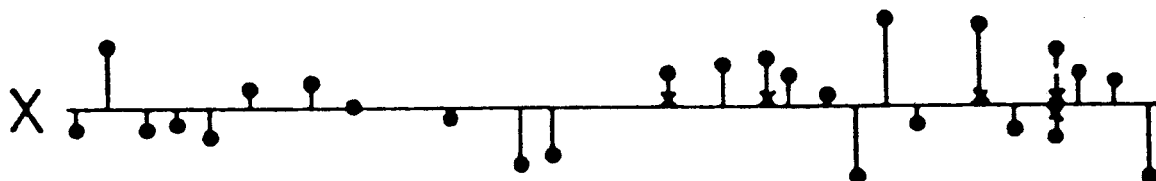
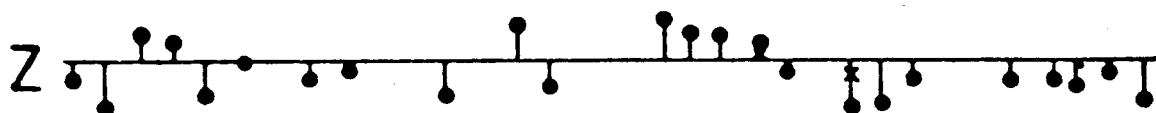
VIEW FROM ABOVE THE MAGNETIC POLE





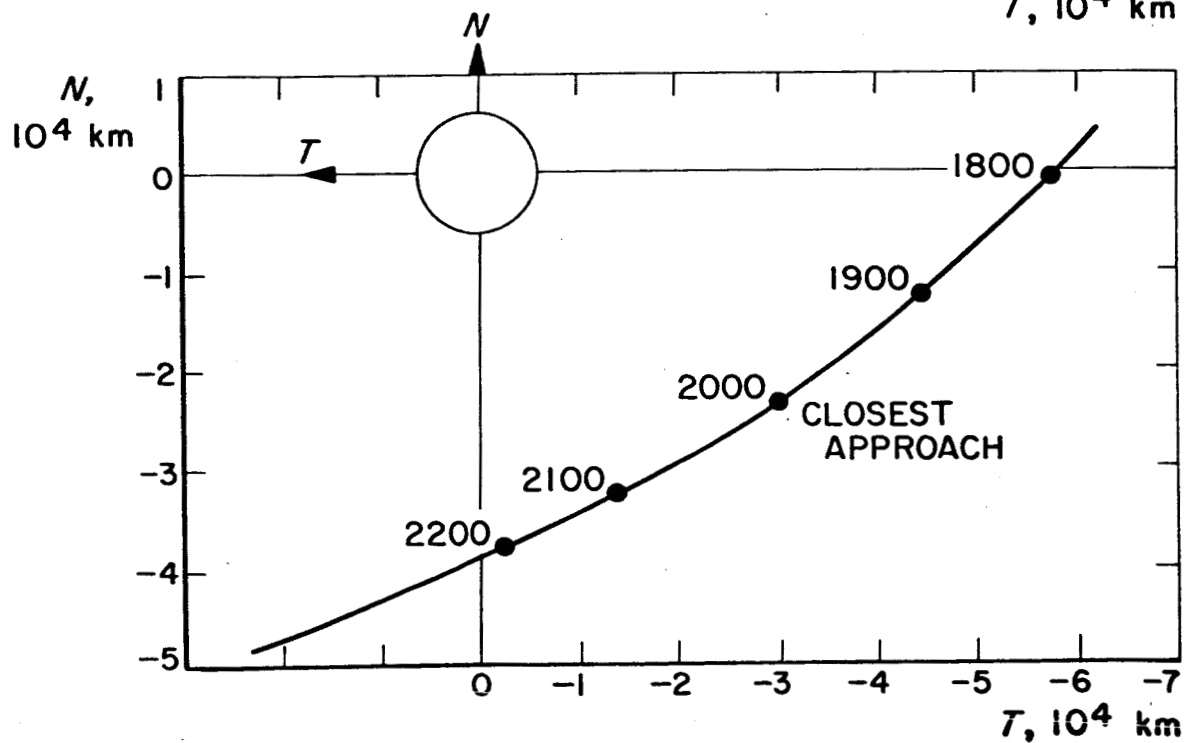
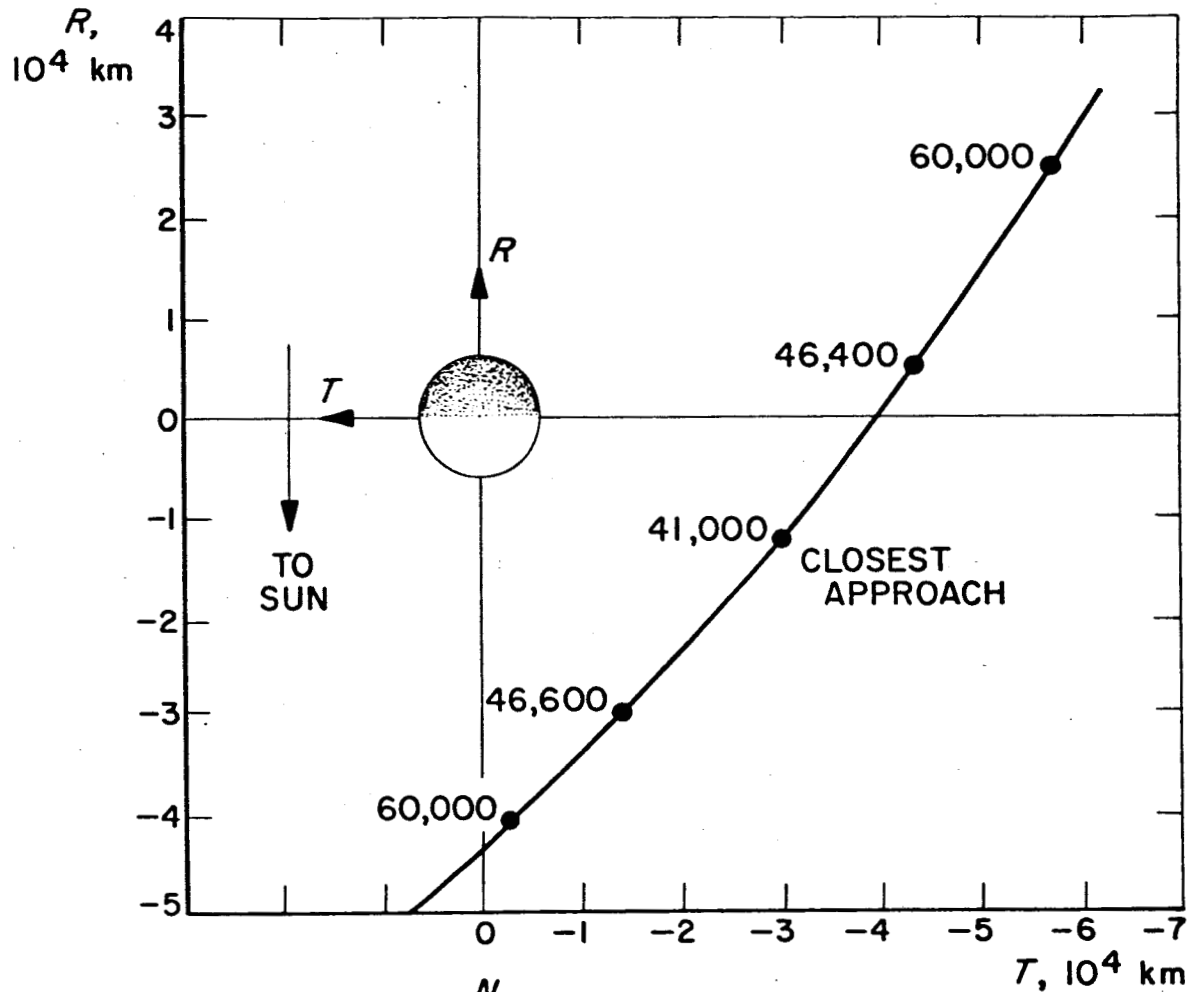


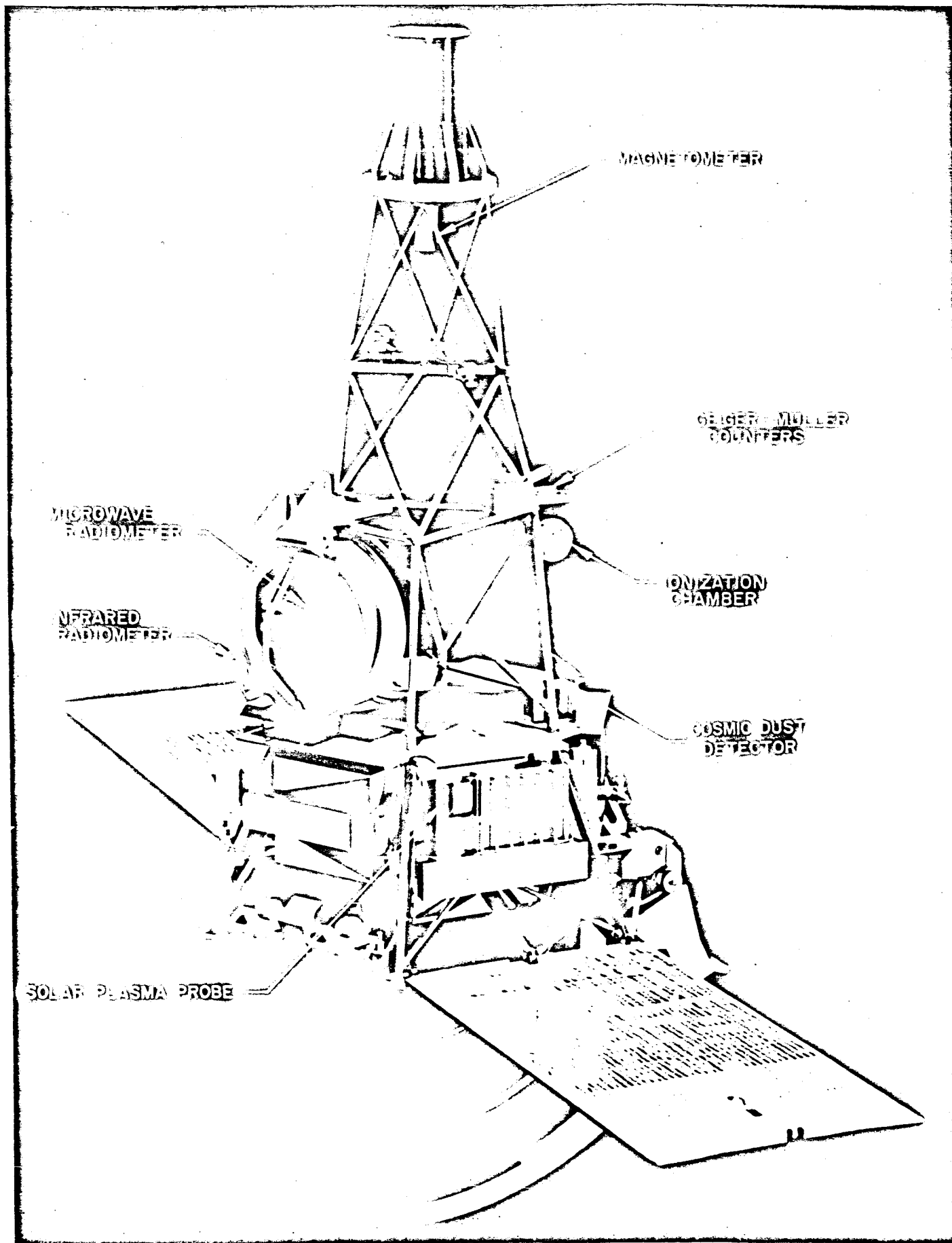
$40^\gamma I$

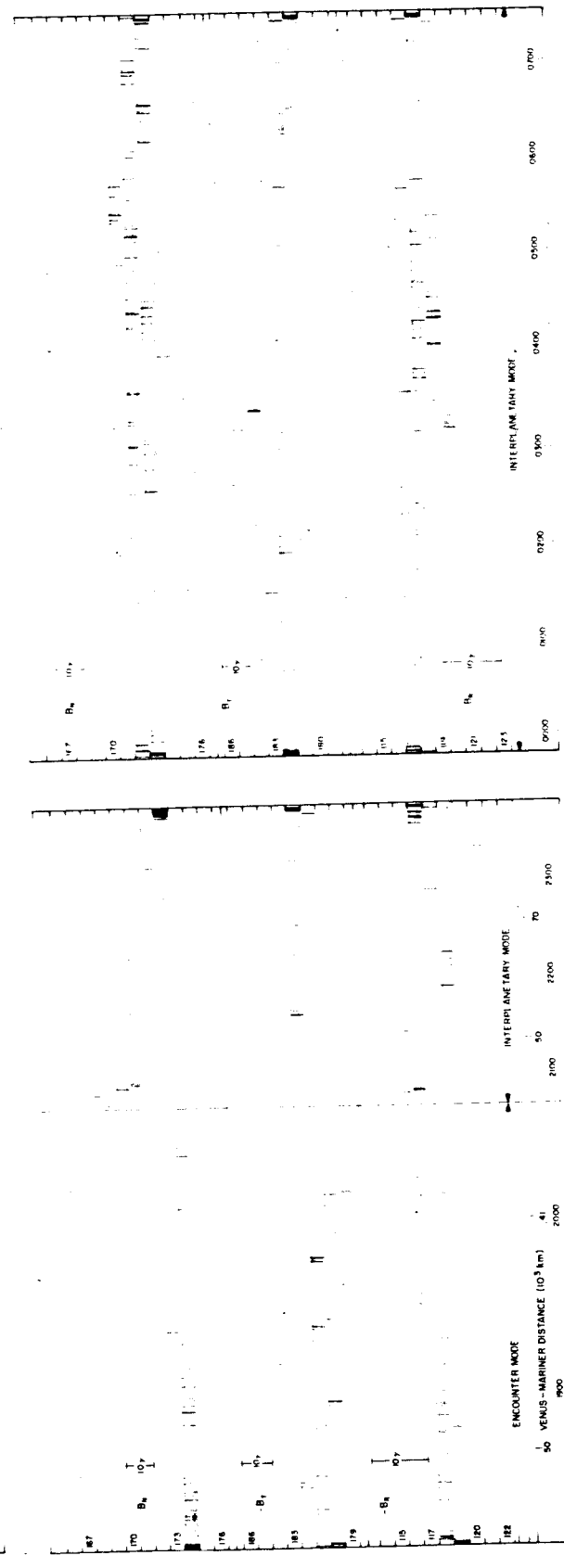
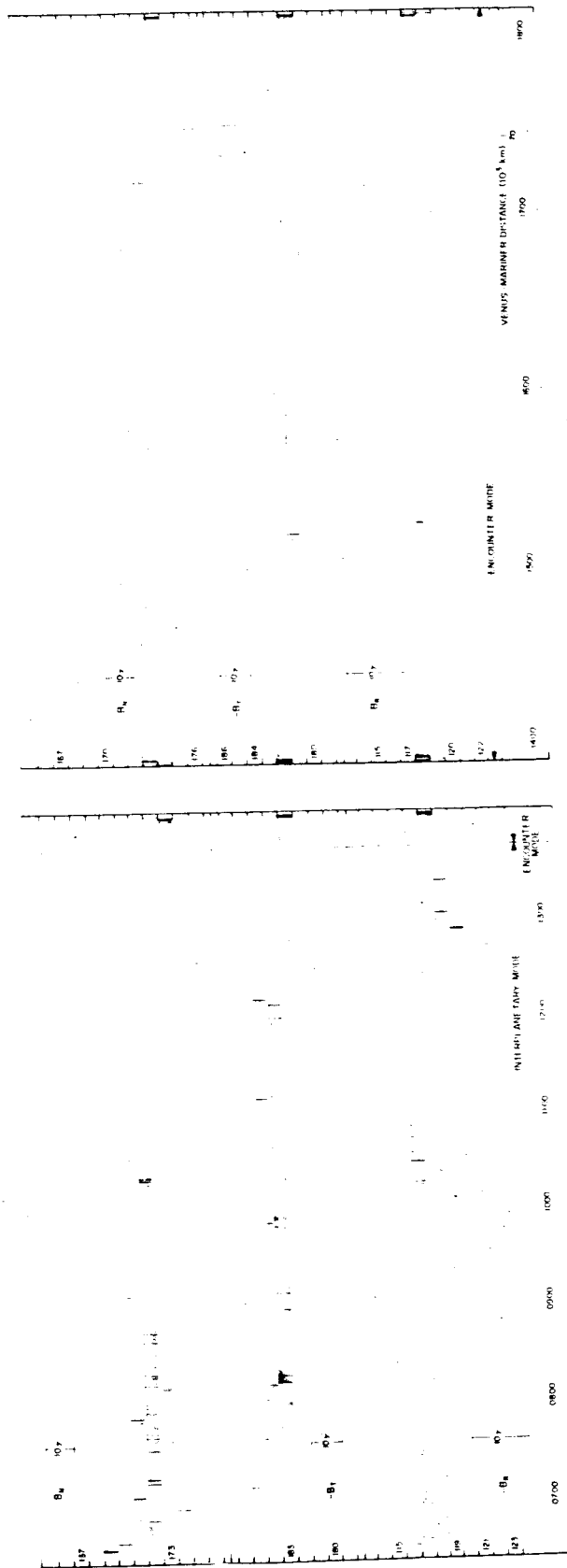


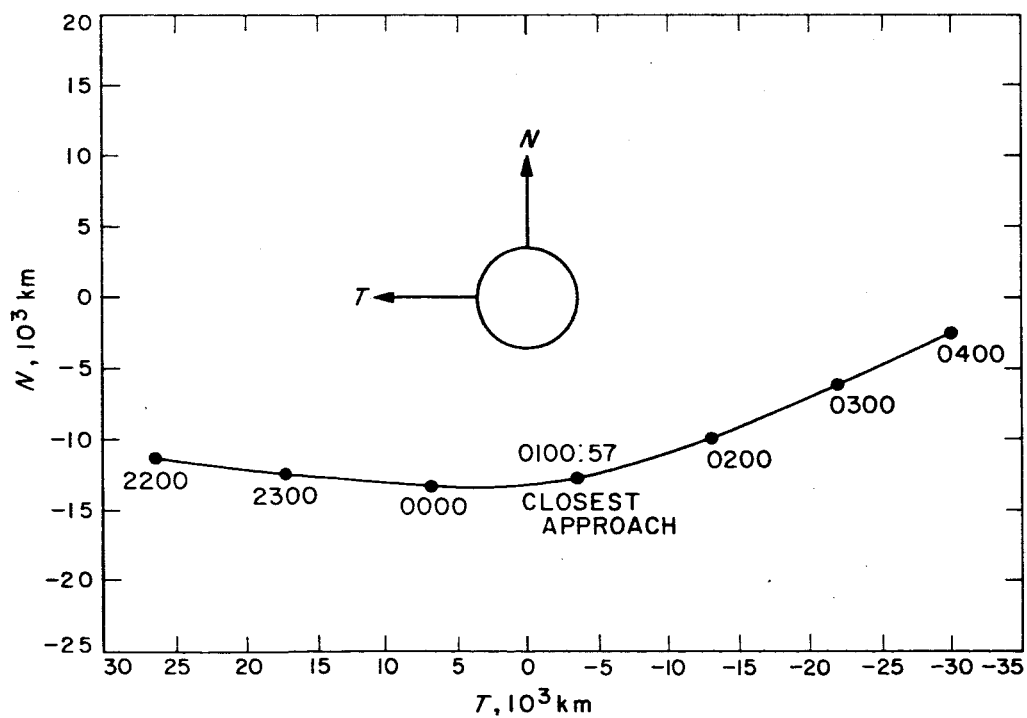
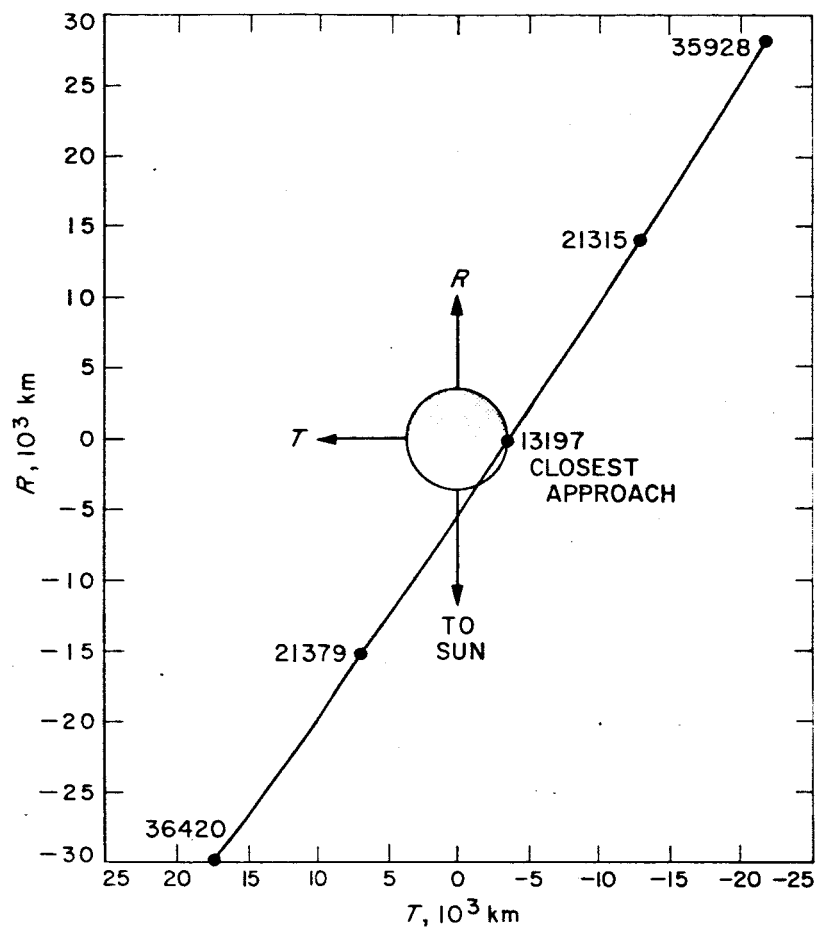
Distance from the surface of the moon

MARINER 2 ENCOUNTER, CAVITY COORDINATES

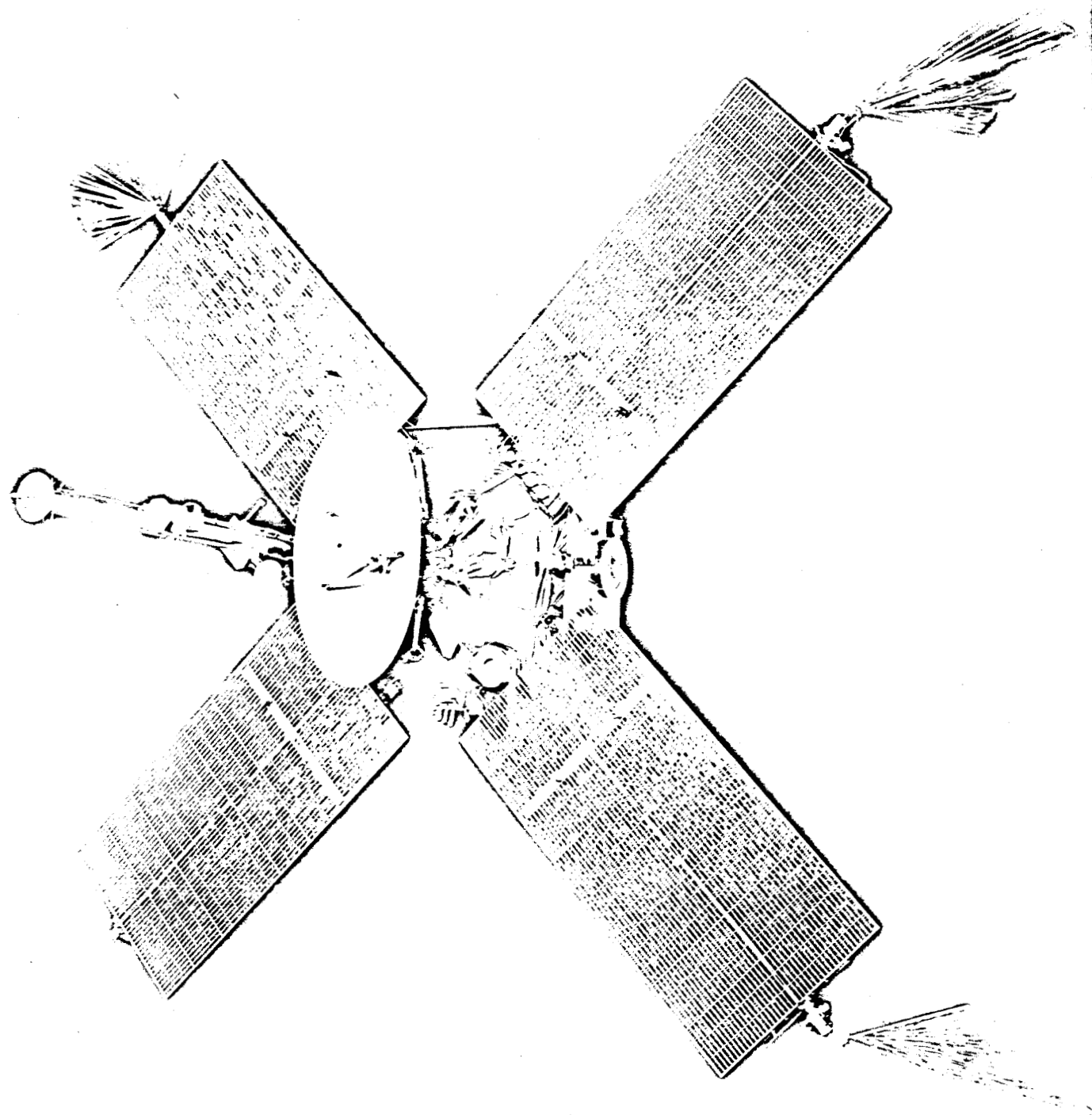


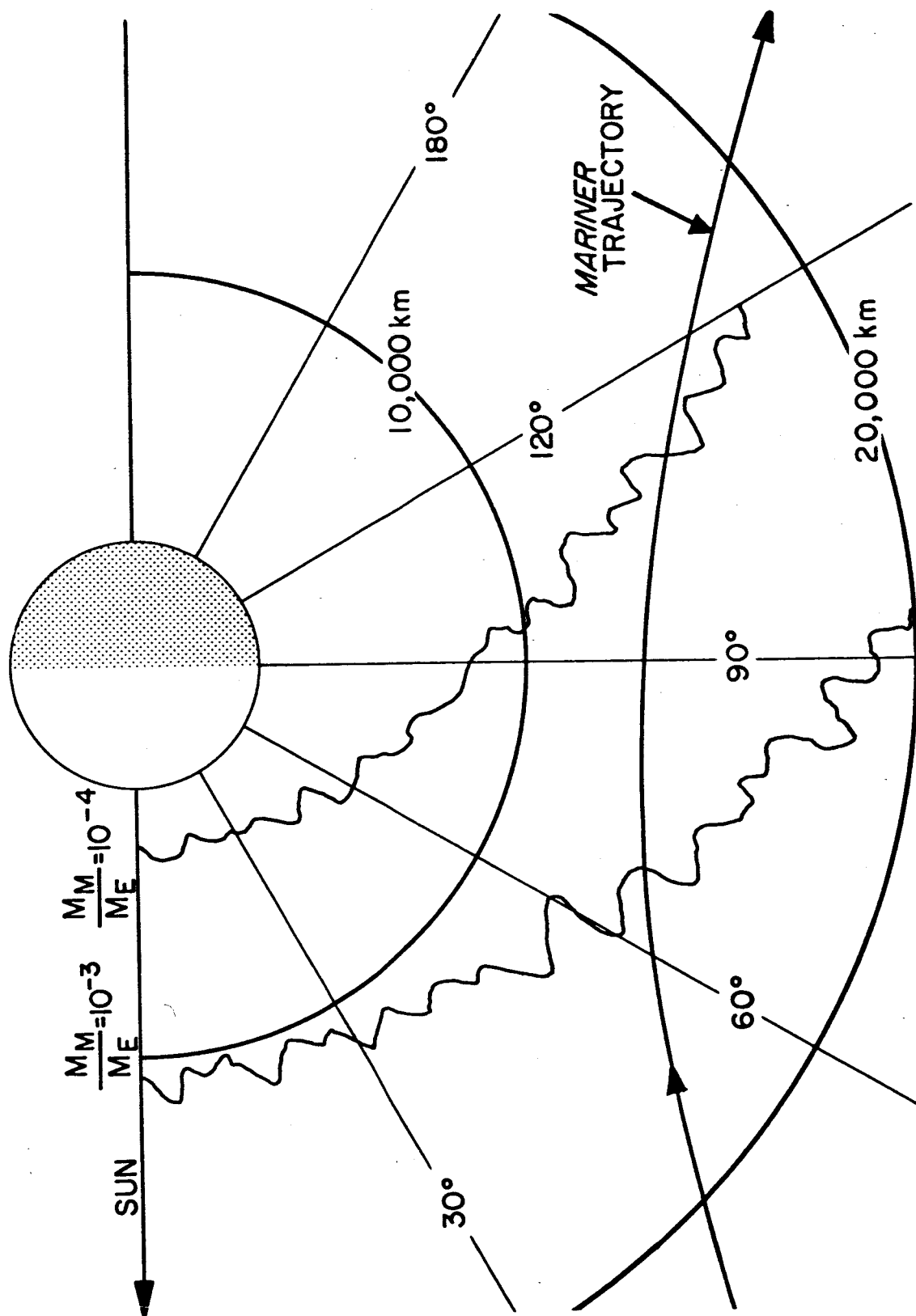






MARINER IV ENCOUNTER





MARINER IV ENCOUNTER, SHOCK FRONT LOCATIONS